J. Phys. B: At. Mol. Opt. Phys. **23** (1990) 2055–2081. Printed in the UK

Medium resolution studies of extreme ultraviolet emission from N_2 by electron impact: the effect of predissociation on the emission cross section of the b $^1\Pi_u$ state

Geoffrey K James†, Joseph M Ajello†, Brian Franklin† and Donald E Shemansky‡

† Jet Propulsion Laboratory, California Institute of Technology, Pasadena, CA 91109, USA

‡ Lunar and Planetary Laboratory, University of Arizona, Tucson, AZ 85712, USA

Received 30 October 1989, in final form 20 February 1990

Abstract. We have measured the electron impact induced fluorescence spectrum of N_2 in the wavelength range 102 to 134 nm at a spectral resolution of 0.05 nm. The experiment was performed in a crossed beam configuration under optically thin conditions. Our spectral measurements provide the emission cross sections of the transitions of the b $^1\Pi_u$–X $^1\Sigma_g^+$ Birge–Hopfield I-band system. The structure and vibrational population distribution of this system are strongly affected by a configuration interaction of the valence b $^1\Pi_u$ and Rydberg c $^1\Pi_u$ and o $^1\Pi_u$ states. Analysis of electron energy loss data shows that these perturbations give rise to excitation cross sections whose v' dependence is strikingly different than the variation of the Franck–Condon factors of the unperturbed diabatic states. A comparison of the excitation and emission cross sections shows that, with the exception of the $v' = 1$ level, the b $^1\Pi_u$ state predissociates with a branching ratio of between 0.95 and 1.00. Predissociation of the b $^1\Pi_u$ state contributes approximately 6% of the total dissociation cross section of N_2 by electron impact at 100 eV. A modified Born approximation analytic model is given for the b $^1\Pi_u$ vibrational excitation cross section. This analysis yields a band system oscillator strength of 0.156.

1. Introduction

As part of a continuing program established to measure absolute emission cross sections of atmospheric species excited by electron impact, we present an analysis of the b $^1\Pi_u$–X $^1\Sigma_g^+$ Birge–Hopfield I-band system of N_2. This work is an extension of the analysis presented in a companion paper for the Rydberg and valence states of N_2 with Σ symmetry (Ajello *et al* 1989).

In a high resolution (0.001 nm) study of b $^1\Pi_u$–X absorption bands Carroll and Collins (1969) observed irregularities in structure and intensity distribution attributed to homogeneous configuration interaction of the b $^1\Pi_u$ state with the first member ($n = 3$) of the c_n $^1\Pi_u$ Rydberg series. Diffuseness in the rotational lines of several bands at lower v' was observed and attributed to predissociation by a triplet state, probably the C′ $^3\Pi_u$ state which goes to the $^4S + {}^2D$ dissociation limit. The effects of vibrational perturbations were also observed in the high resolution (10 meV) electron energy loss experiments of Geiger and Schröder (1969). The measured intensity distribution within the b $^1\Pi_u$ progression ($v' = 0$–16) showed striking deviations

0953-4075/90/122055+27$03.50

from the unperturbed intensity distribution based on calculated Franck–Condon factors. A quantitative analysis of the interaction of the valence b $^1\Pi_u$ and Rydberg c $^1\Pi$ and o $^1\Pi$ states was performed by Stahel *et al* (1983) based on vibronic interaction matrix optimisation as well as on direct solutions of coupled oscillator equations. Diabatic and adiabatic potential functions for the $^1\Pi_u$ states were also calculated.

The EUV emission spectrum of N_2 produced by a low pressure discharge lamp was recently measured by Roncin *et al* (1987, 1989) at high resolution (0.0008 nm), providing identifications of the emission (excluding resonance bands $(v',0)$) from the five Rydberg and valence states (c_4', b' $^1\Sigma_u^+$ and b, c_3, o_3 $^1\Pi_u$).

In the present work we extend our earlier measurements of the EUV emission spectrum of N_2 induced by electron impact at 20 and 100 eV (Ajello *et al* 1989) to cover the wavelength range 102 to 134 nm. The spectral measurements provide the emission cross sections of the transitions of the b $^1\Pi_u$–X $^1\Sigma_g^+$ band system, together with many dominant atomic dissociation fragments (N I, N II). The measured emission cross sections of transitions of the c_4' $^1\Sigma_u^+$–X $^1\Sigma_g^+$ and b' $^1\Sigma_u^+$–X $^1\Sigma_g^+$ band systems in this wavelength range were presented by Ajello *et al* (1989). In addition, we have measured the excitation function (0–400 eV) for the b–X (1,2) transition and applied a modified Born approximation analytic model to calculate the oscillator strength for the b $^1\Pi_u$ –X band system.

Comparison of the experimental emission cross sections presented in this work with excitation cross sections from electron energy loss experiments (Zipf and Gorman 1980, Lassettre 1974) provides an estimate of predissociation and emission yields. With the exception of the the $v' = 1$ level, vibrational levels of the b $^1\Pi_u$ state predissociate with a branching ratio of between 0.95 and 1.00. Predissociation of the b $^1\Pi_u$ state contributes approximately 6% of the total dissociation cross section of N_2 by electron impact at 100 eV (Winters 1965).

Previous electron impact studies of the EUV emission spectrum of N_2 (Zipf and Gorman 1980, Morgan and Mentall 1983, Zipf and McLaughlin 1978, Aarts and De Heer 1971, Huschilt *et al* 1981, Forand *et al* 1988) have lead to misinformation concerning identifications as well as cross sections and predissociation rates, as discussed by Ajello *et al* (1989). The present measurements are made with higher resolution (0.05 nm), lower foreground abundance and more accurate calibration standards than the previous work.

2. Experimental apparatus

The experimental apparatus and calibration techniques have been described in detail in earlier publications (Ajello *et al* 1988, 1989, Ajello and Shemansky 1985, Shemansky *et al* 1985a). In brief, the instrument consists of an electron impact collision chamber in tandem with a UV spectrometer. A magnetically collimated beam of electrons (2–400 eV) is crossed under optically thin conditions with a beam of N_2 gas formed by a capillary array. Emitted photons are detected at 90° by a commercial 1.0 m monochromator equipped with both channeltron and photomultiplier detectors to cover the wavelength range 102–134 nm studied in the present work.

The calibration procedure reflects the revised benchmark cross section for Lyman-α production by dissociative excitation of H_2 (Ajello *et al* 1988). The root sum square uncertainty for the absolute cross sections given in this work is estimated to be 22% based on the uncertainties in the revised Lyman-α cross section, relative calibration and signal statistics (Ajello *et al* 1989).

3. Medium resolution spectral data

Figures 1 and 2 show the calibrated optically thin emission spectrum of N_2 from 102 to 123 nm induced by electron impact at 100 eV measured at a resolution of 0.05 nm (6 meV). Spectral features are labelled using an extension of the numbering system of Ajello *et al* (1989); wavelength intervals numbered 27 through 39 are subdivided into observed features identified by a letter. The transitions within the $b\,^1\Pi_u$–$X\,^1\Sigma_g^+$ $v' = 1$ progression are indicated in the figures. In addition, the spectrum from 102 to 111 nm at 20 eV electron impact energy is shown in figure 3. Measuring the spectrum at 20 eV impact energy, below the threshold for dissociative excitation of N I lines, enables us to unambiguously identify the many N I and N II features which contribute to the spectrum observed at 100 eV.

The emission cross sections at 20, 100 and 200 eV for each of the observed features are listed in table 1, together with identifications of the blended spectral components. The 200 eV measurements are taken from the spectra presented by Ajello *et al* (1989) at low resolution (0.5 nm). The N_2 band origins are from Roncin *et al* (1987) for $v'' \neq 0$. Resonance transitions from the principal Rydberg and valence states of N_2 are not observed in this wavelength range. Identification of the $b\,^1\Pi_u$– $X\,^1\Sigma_u^+$ $v' = 1$ progression is made using the data of Zipf and Gorman (1980). The many N I and

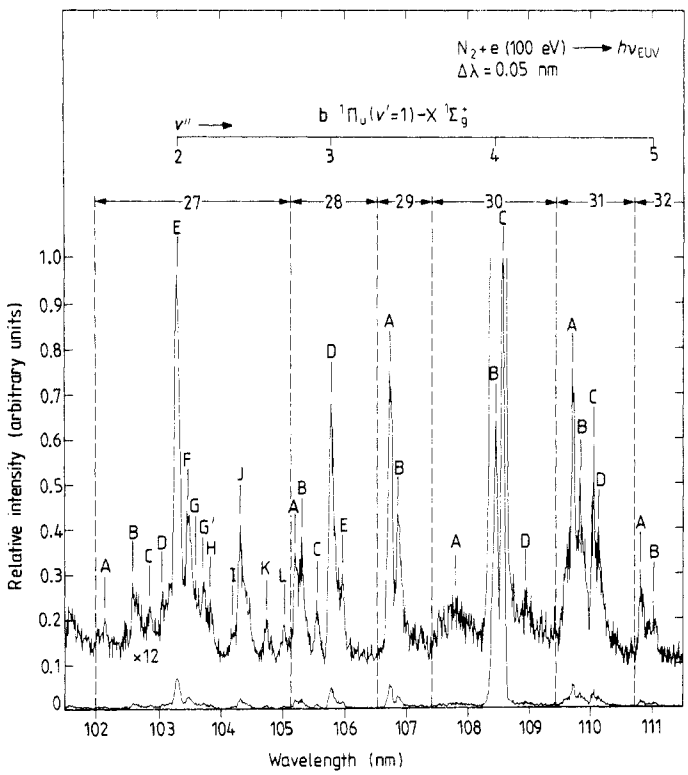

Figure 1. Calibrated optically thin emission spectrum of N_2 from 102 to 111 nm produced by electron impact at 100 eV, measured at 0.05 nm resolution. The $b\,^1\Pi_u$ ($v' = 1$)–$X\,^1\Sigma_g^+$ progression ($v'' = 2$–5) is identified. The feature numbers are listed in table 1, together with spectroscopic assignments and emission cross sections.

Table 1. Emission cross section of N_2 at 20, 100 and 200 eV. The abbreviated table headings are as follows: λ, wavelength; λ_{OP}, observed peak wavelength; $(\Delta\lambda)_{int}$, integrated wavelength interval; Q_{em}, emission cross section; OM, other measurements.

Feature	Species	λ (nm)	Term	λ_{OP} (nm)	$(\Delta\lambda)_{int}$ (nm)	Q_{em} (10^{-19} cm^2) 200 eV	100 eV	20 eV	OM (10^{-19} cm^2) 200 eV (100 eV)
27					102.0–105.16	5.5	6.00	2.29	
A				102.15	102.0–102.22		0.26	—	
B	N_2	102.649[a]	c_4' (0,3) s	102.59	102.52–102.81		0.52	0.17	
	N_2	102.689[a]	c_3 (1,4)						
C	N_2	102.859[a]	c_4' (1,4) s	102.87	102.81–103.02		0.32	—	
	N I	102.868	$^2D^o$–^2D						
	N_2	102.900[a]	c_4' (2,5) s						
	N I	102.950	$^2D^o$–^2F						
	N_2	102.979[a]	c_4' (3,6)						
D	N_2	103.027[a]	c_4' (4,7)	103.07	103.02–103.15		0.27	—	
	N I	103.0446	$^2D^o$–^2S						
	N I	103.076	$^2D^o$–^2D						
	N_2	103.136[a]	b (7,4)						
E	N I	103.162	$^2D^o$–^2F	103.30	103.15–103.45		1.93	1.13	1.34[b] b (1,2)
	N I	103.218	$^2D^o$–^2P						1.27[c] b (1,2)
	N_2	103.229[a]	c_4' (6,9)						(2.11)[b] b (1,2)
	N_2	103.283[a]	b (1,2) s						
	N I	103.342	$^2D^o$–^2D						
	N I	103.370	$^2D^o$–^2D						
	N_2	103.390[a]	b′ (3,4)						
	N I	103.437	$^2D^o$–^2F						
F	N I	103.467	$^2D^o$–^4P	103.47	103.45–103.57		0.57	0.33	
	N_2	103.470[a]	b′ (9,6) s						
	N_2	103.482[a]	b′ (6,5) vw						
	N I	103.500	$^2D^o$–^2P						

G	N_2	103.589[a]	b′ (12,7)	103.59	103.57 – 103.64		0.20	0.15
G′	N I	103.7382	$^2D^o$–^2F	103.72	103.64–103.77		0.34	—
	N I	103.764	$^2D^o$–^2D					
H	N I	103.828	$^2D^o$–^4F	103.84	103.77–103.99		0.30	0.13
	N I	103.8366	$^2D^o$–^2F					
	N I	103.873	$^2D^o$–^4F					
	N I	103.890	$^2D^o$–^2P					
	N_2	103.955[a]	b (6,4) vw					
I	N_2	104.171[a]	b′ (8,6)	104.20	104.15–104.25		0.12	0.06
	N_2	104.205[a]	b′ (5,5)					
J	N_2	104.303[a]	b′ (11,7)	104.32	104.25–104.63		0.78	0.10
	N I	104.3080	$^2D^o$–^4D					
	N I	104.3166	$^2D^o$–^2F					
	N I	104.3739	$^2D^o$–^2P					
	N I	104.3845	$^2D^o$–^2P					
	N I	104.3991	$^2D^o$–^4P					
	N I	104.4069	$^2D^o$–^4F					
	N I	104.4087	$^2D^o$–^2P					
	N I	104.4171	$^2D^o$–^2F					
	N I	104.4188	$^2D^o$–^2P					
	N I	104.4606	$^2D^o$–^2P					
	N I	104.4633	$^2D^o$–^4F					
K	N_2	104.658[a]	b (5,4)	104.74	104.63–104.89		0.20	0.14
	N_2	104.741[a]	o_3 (4,8) w					
	N_2	104.819[a]	b′ (7,6) vw					
L	N_2	105.069[a]	c_4' (0,4) s	105.02	104.89–105.16		0.22	0.08
28					105.16–106.57	2.7	2.38	1.12
A	N I	105.1868	$^2D^o$–^2D	105.20	105.16–105.26		0.32	0.03
	N I	105.1956	$^2D^o$–^2D					
	N I	105.2082	$^2D^o$–^4D					

Table 1. (Continued)

Feature	Species	λ (nm)	Term	λ_{OP} (nm)	$(\Delta\lambda)_{int}$ (nm)	Q_{em} (10^{-19} cm^2) 200 eV	100 eV	20 eV	OM (10^{-19} cm^2) 200 eV (100 eV)
A	N I	105.2215	$^2D^\circ$–^2F						
	N_2	105.257[a]	c_4' (1,5) s						
B	N_2	105.268[a]	c_4' (2,6) s	105.30	105.26–105.46		0.48	0.09	
	N I	105.2834	$^2D^\circ$–^2P						
	N I	105.2909	$^2D^\circ$–^4P						
	N I	105.3088	$^2D^\circ$–^4P						
	N_2	105.318[a]	c_4' (3,7) s						
	N I	105.3184	$^2D^\circ$–^2P						
	N I	105.3184	$^2D^\circ$–^4F						
	N I	105.3231	$^2D^\circ$–^2P						
	N I	105.333	$^2D^\circ$–^2P						
	N_2	105.337[a]	c_4' (4,8)						
	N I	105.3496	$^2D^\circ$–^4P						
	N I	105.3656	$^2D^\circ$–^4F						
	N I	105.3744	$^2D^\circ$–^4F						
	N I	105.3988	$^2D^\circ$–^2P						
	N I	105.4333	$^2D^\circ$–^4P						
	N I	105.4430	$^2D^\circ$–^4P						
C	N_2	105.544[a]	b (7,5)	105.56	105.46–105.68		0.22	0.18	
D	N_2	105.763[a]	b (1,3)	105.79	105.68–105.93		1.11	0.67	0.86[b] b (1,3)
	N_2	105.814[a]	b′(3,5) s						(1.39)[b] b (1,3)
	N_2	105.830[a]	b′(9,7)						
E				105.97	105.93–106.04		0.25	0.07	
F	N II	106.3350	$^3P^\circ$–^3P	106.43	106.29–106.57		—	0.07	
	N II	106.3362	$^3P^\circ$–^3P						
	N_2	106.401[a]	b (5,6) vw						

F	N II	106.4142	$^3P^o$–^3P					
	N II	106.4153	$^3P^o$–^3P					
	N II	106.4220	$^3P^o$–^3P					
	N II	106.4443	$^3P^o$–^3P					
	N II	106.4947	^1D–$^3P^o$					
	N II	106.4958	^1D–$^3P^o$					
29					106.57–107.42	2.6	1.70	0.19
A	N_2	106.671[a]	b′(11,8) s	106.73	106.65–106.08		0.96	0.11
	N I	106.6992	$^2D^o$–^2D					
	N I	106.7092	$^2D^o$–^2D					
	N I	106.7206	$^2D^o$–^2D					
	N I	106.7308	$^2D^o$– ^2D					
	N I	106.7386	$^2D^o$– ^4D					
	N I	106.7399	$^2D^o$–^4D					
	N I	106.7493	$^2D^o$–^4D					
	N I	106.7616	$^2D^o$–^2F					
	N II	106.7877	$^3P^o$–^3D					
	N I	106.7953	$^2D^o$–^4P					
B	N I	106.8221	$^2D^o$–^4P	106.86	106.80–107.06		0.74	0.08
	N I	106.8321	$^2D^o$–^4P					
	N I	106.8376	$^2D^o$–^4P					
	N I	106.8477	$^2D^o$–^4P					
	N I	106.8512	$^2D^o$–^2F					
	N I	106.8612	$^2D^o$–^2F					
	N I	106.8644	$^2D^o$–^2P					
	N I	106.8668	$^2D^o$–^2P					
	N I	106.8681	$^2D^o$–^4F					
	N II	106.8962	$^3P^o$–^3D					
	N I	106.9110	$^2D^o$–^4F					
	N I	106.9206	$^2D^o$–^4F					
	N I	106.9374	$^2D^o$–^2P					
	N I	106.9468	$^2D^o$–^2P					
	N II	106.9626	$^3P^o$–^3D					

Table 1. (Continued)

Feature	Species	λ (nm)	Term	λ_{OP} (nm)	$(\Delta\lambda)_{int}$ (nm)	Q_{em} (10^{-19} cm^2) 200 eV	100 eV	20 eV	OM (10^{-19} cm^2) 200 eV (100 eV)
B	N I	106.9990	$^2D^\circ$–^2P						
	N I	107.0012	$^2D^\circ$–^4P						
	N I	107.0111	$^2D^\circ$–^4P						
30					107.42–109.40	23.7	28.05	0.82	
A	N_2	107.573[a]	c_4' (0,5)	107.84	107.42–108.22		1.17	0.35	
	N_2	107.714[a]	c_4' (2,7)						
	N_2	107.733[a]	c_4' (3,8) w						
	N_2	107.736[a]	c_4' (1,6)						
B	N_2	108.3167[d]	b′ (3,6)	108.46	108.23–108.51		11.8	0.36	0.38[b] b (1,4)
	N_2	108.322[e]	b′ (0,5)						(0.56)[b] b (1,4)
	N_2	108.338[f]	b (1,4)						
	N II	108.3990	g^3P–$^3D^\circ$						
	N II	108.4562	g^3P–$^3D^\circ$						
	N II	108.4580	g^3P–$^3D^\circ$						
C	N II	108.5529	g^3P–$^3D^\circ$	108.57	108.51–108.73		14.6	—	
	N II	108.5546	g^3P–$^3D^\circ$						
	N II	108.5701	g^3P–$^3D^\circ$						
D				108.96	108.83–109.09		0.48	0.10	
31					109.40–110.72	2.7	3.18	0.15	
A	N I	109.5942	$^2D^\circ$–^2D	109.70	109.54–109.77		1.21	—	
	N I	109.6046	$^2D^\circ$–^2D						
	N I	109.6220	$^2D^\circ$–^2D						
	N I	109.6325	$^2D^\circ$–^2D						
	N I	109.6749	$^2D^\circ$–^4D						
	N I	109.6769	$^2D^\circ$–^4D						

A	N I	109.6874	$^2D^o$–^4D						
	N I	109.6945	$^2D^o$–^4D						
	N I	109.7237	$^2D^o$–^2F						
	N_2	109.7440[d]	b′ (7,8)						
	N I	109.7492	$^2D^o$–^4P						
B	N I	109.7716	$^2D^o$–^4P	109.82	109.77–109.96		0.82	—	
	N I	109.7821	$^2D^o$–^4P						
	N I	109.7995	$^2D^o$–^4P						
	N I	109.8097	$^2D^o$–^4P						
	N I	109.8261	$^2D^o$–^2F						
	N I	109.8625	$^2D^o$–^4F						
	N I	109.8759	$^2D^o$–^2P						
	N I	109.8952	$^2D^o$–^2P						
	N I	109.9042	$^2D^o$–^4F						
	N I	109.9150	$^2D^o$–^4F						
	N I	109.9263	$^2D^o$–^4F						
C	N I	110.03593	$^2D^o$–^2P	110.05	109.97–110.09		0.56	0.05	
	N I	110.04649	$^2D^o$–^2P						
	N_2	110.048[f]	b′ (1,6)						
D	N I	110.12910	$^2D^o$–^2P	110.11	110.09–110.34		0.60	0.10	
	N I	110.2509	$^2D^o$–^4P						
	N I	110.3362	$^2D^o$–^4P						
32					110.72–112.97	0.94	0.98	0.50	
A	N_2	110.787[f]	b′ (9,9)	110.81	110.72–110.97		0.39	0.24	
	N_2	110.908[e]	b′ (6,8)						
	N_2	110.910[f]	b′ (3,7)						
B	N_2	110.9962[d]	b (1,5)	111.02	110.98–111.12		0.17	0.14	0.09[b] b (1,5) (0.15)[b] b (1,5)
C	N_2	111.800[f]	b′ (2,7)	111.90	111.89–111.99		0.07	—	

Table 1. (Continued)

Feature	Species	λ (nm)	Term	λ_{OP} (nm)	$(\Delta\lambda)_{int}$ (nm)	Q_{em} (10^{-19} cm^2) 200 eV	100 eV	20 eV	OM (10^{-19} cm^2) 200 eV (100 eV)
D	N_2	112.724[f]	b′ (1,7)	112.75	112.68–112.83		0.20	0.05	
E				112.88	112.83–112.97		0.17	0.07	
33					112.97–114.28	6.4	7.2	0.17	
A	N I	113.41651	g^4S^o–^4P	113.48	113.35–113.59		7.2	0.17	
	N I	113.44147	g^4S^o–^4P						
	N I	113.49801	g^4S^o–^4P						
	N_2	113.583[e]	b′ (3,8)						
34					114.28–115.78	2.8	1.70	0.28	
A	N I	114.331	$^2P^o$–^2P	114.37	114.28–114.43		0.66	0.06	
	N I	114.36458	$^2P^o$–^2S						
	N I	114.36508	$^2P^o$–^2S						
	N I	114.416	$^2P^o$–^2D						
B	N I	114.877	$^2P^o$–^2P	114.925	114.87–114.99		0.39	—	
	N I	114.939	$^2P^o$–^2P						
C	N I	115.215	$^2P^o$–^2D	115.23	115.14–115.28		0.13	—	
	N I	115.263	$^2P^o$–^2D						
D	N I	115.3453	$^2P^o$–^2P	115.32	115.28–115.38		0.10	0.04	
E	N_2	115.492[e]	b′ (1,8)	115.55	115.46–115.63		0.24	0.10	
F				115.66	115.63–115.78		0.19	0.08	

35					115.78–117.57	7.2	6.2	0.06	
A	N I	115.9193	$^2P^o$–^2D	115.93	115.85–115.99		0.13	—	
	N I	115.9273	$^2P^o$–^2D						
	N I	115.9344	$^2P^o$–^4D						
	N I	115.98172	g^4S^o–^2P						
B	N I	116.0171	$^2P^o$–^2P	116.06	116.00–116.20		0.17	0.06	
	N I	116.039	$^2P^o$–^4P						
	N I	116.0476	$^2P^o$–^2P						
	N I	116.0713	$^2P^o$–^2P						
	N I	116.09370	g^4S^o–^2P						
	N I	116.1118	$^2P^o$–^2P						
C	N I	116.38835	$^2D^o$–^2D	116.42	116.32–116.49		1.05	—	
	N I	116.40016	$^2D^o$–^2D						
	N I	116.42064	$^2D^o$–^2D						
	N I	116.43246	$^2D^o$–^2D						
	N_2	116.490[e]	b′ (0,8)						
D	N I	116.55943	$^2D^o$–^4D	116.58	116.49–116.64		0.19	—	0.034[b] b (1,7)
	N I	116.5717	$^2D^o$–^4D						(0.051)[b] b (1,7)
	N I	116.58358	$^2D^o$–^4D						
	N I	116.6003	$^2D^o$–^4D						
	N_2	116.62[g]	b (1,7)						
E	N I	116.74484	$^2D^o$–^2F	116.74	116.67–116.80		2.26	—	
	N I	116.7502	$^2D^o$–^4P						
	N I	116.7743	$^2D^o$–^4P						
	N I	116.7862	$^2D^o$–^4P						
F	N I	116.82154	$^2D^o$–^4P	116.85	116.80–116.93		1.61	—	
	N I	116.83344	$^2D^o$–^4P						
	N I	116.84167	$^2D^o$–^2F						
	N I	116.85358	$^2D^o$–^2F						
G	N I	116.96933	$^2D^o$–^4F	117.00	116.93–117.24		0.79	—	
	N I	117.01572	$^2D^o$–^4F						
	N I	117.0220	$^2P^o$–^2D						

Table 1. (Continued)

Feature	Species	λ (nm)	Term	λ_{OP} (nm)	$(\Delta\lambda)_{int}$ (nm)	Q_{em} (10^{-19} cm^2) 200 eV	100 eV	20 eV	OM (10^{-19} cm^2) 200 eV (100 eV)
G	N I	117.02766	$^2D^o$–^4F						
	N I	117.04165	$^2D^o$–^4F						
	N I	117.0432	$^2P^o$–^2D						
	N I	117.0485	$^2P^o$–^4D						
	N I	117.0499	$^2P^o$–^4D						
	N I	117.0536	$^2D^o$–^4F						
	N I	117.06743	$^2D^o$–^2P						
	N I	117.0815	$^2P^o$–^4P						
	N I	117.10834	$^2D^o$–^2P						
	N I	117.1418	$^2P^o$–^2P						
	N I	117.1502	$^2P^o$–^4P						
	N I	117.1722	$^2P^o$–^2P						
	N I	117.1904	$^2P^o$–^2P						
	N I	117.242	$^2P^o$–^4F						
36					117.57–118.62	2.23	3.57	0.11	
A	N I	117.65097	$^2D^o$–^2P	117.64	117.57–117.71		1.89	—	
	N I	117.66304	$^2D^o$–^2P						
B	N I	117.76948	$^2D^o$–^2P	117.76	117.71–117.84		1.07	—	
C	N I	118.3278	$^2D^o$–^4P	118.43	118.36–118.48		0.33	0.05	
	N I	118.3400	$^2D^o$–^4P						
	N_2	118.362[e]	b′ (1,9)						
	N I	118.4235	$^2D^o$–^4P						
	N I	118.4357	$^2D^o$–^4P						
D	N I	118.4984	$^2D^o$–^4P	118.55	118.48–118.62		0.28	0.07	

37					118.62–119.53	< 1.0	0.79	0.08	
A	N I	118.8971	$^2P^o$–^2D	118.89	118.81–119.05		0.58	0.08	
	N I	118.9249	$^2P^o$–^2D						
	N I	119.0031	$^2P^o$–^4P						
	N I	119.0494	$^2P^o$–^4P						
B	N I	119.0688	$^2P^o$–^4P	119.09	119.05–119.19		0.21	—	
	N I	119.0855	$^2P^o$–^2F						
	N I	119.0923	$^2P^o$–^2P						
	N I	119.1019	$^2P^o$–^2P						
	N I	119.1603	$^2P^o$–^4F						
	N I	119.1925	$^2P^o$–^2P						
38					119.53–121.58	31.1	38.77	0.28	(40.0)[h]
A	N_2	119.59	b (1,8)[g]	119.62	119.53–119.68		0.16	0.08	0.10[b] b (1,8) (0.14)[b] b (1,8)
B	N I	119.95490	g^4S^o–^4P	119.95	119.86–120.13		38.0	0.08	
	N I	120.02238	g^4S^o–^4P						
	N I	120.07113	g^4S^o–^4P						
C	N_2	121.335[e]	b′ (1,10)	121.41	121.31–121.46		0.30	0.07	
D				121.53	121.46–121.58		0.31	0.06	
39					121.58–122.60		0.55	—	
A				122.50	122.44–122.60		0.55	—	

[a] Intensity of discharge measurement (Roncin *et al* 1987): s, strong; w, weak; vw, very weak.
[b] Zipf and Gorman (1980), cross section corrected as indicated in text by a factor of 0.597. Measurement interval unknown.
[c] Morgan and Mentall (1983), cross section corrected as indicated in text by factor of 0.607. Measurement interval unknown.
[d] Tilford and Wilkinson (1964).
[e] Wilkinson and Houk (1956).
[f] Roncin *et al* (1989) and private communication.
[g] Birge and Hopfield (1928) + 0.02 nm.
[h] Ajello and Shemansky (1985), cross section corrected as indicated in text by a factor of 0.893.

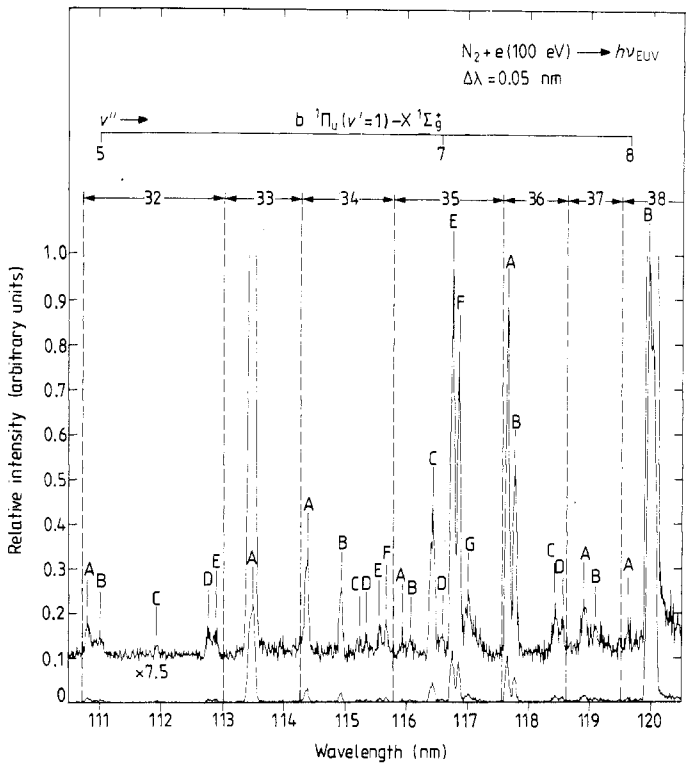

Figure 2. Calibrated optically thin emission spectrum of N_2 from 111 to 120 nm produced by electron impact at 100 eV, measured at 0.05 nm resolution. The b $^1\Pi_u$ ($v' = 1$)–X $^1\Sigma_g^+$ progression ($v'' = 5, 7, 8$) is indicated.

N II multiplets are assigned using the compilation by Kelly (1987). Emission cross sections measured by Zipf and Gorman (1980) and Morgan and Mentall (1983) for the b $^1\Pi_u$– X $^1\Sigma_g^+$ $v' = 1$ progression are also listed. These previous measurements were hampered by erroneous calibration standards available at the time. Corrections to their published values have been made which reflect the revised benchmark cross section for Lyman-α production by dissociative excitation of H_2 measured in this laboratory (Ajello *et al* 1988). The relative intensities observed in the discharge measurements of Roncin *et al* (1987) for the non-resonance transitions are also noted since the discharge lamp and electron impact band intensities are correlated.

The spectra in figures 1–3 were obtained using a channeltron detector which has diminished sensitivity above 120 nm. In order to extend observations of the $v' = 1$ progression of the b $^1\Pi_u$– X $^1\Sigma_g^+$ band system to $v'' > 8$ the emission spectrum of N_2 from 116 to 134 nm at 100 eV impact energy and 0.05 nm resolution was obtained using a photomultiplier detector with a CsTe photocathode (figure 4). The $v' = 1$ progression is identified up to $v'' = 12$, together with the LBH bands and N I multiplets in this spectral region (Ajello and Shemansky 1985).

The excitation function (0–400 eV) for the strongest b–X (1,2) transition of the Birge–Hopfield I system at 103.28 nm measured at 0.086 nm resolution is shown in figure 5, overplotted with the data of Zipf and Gorman (1980).

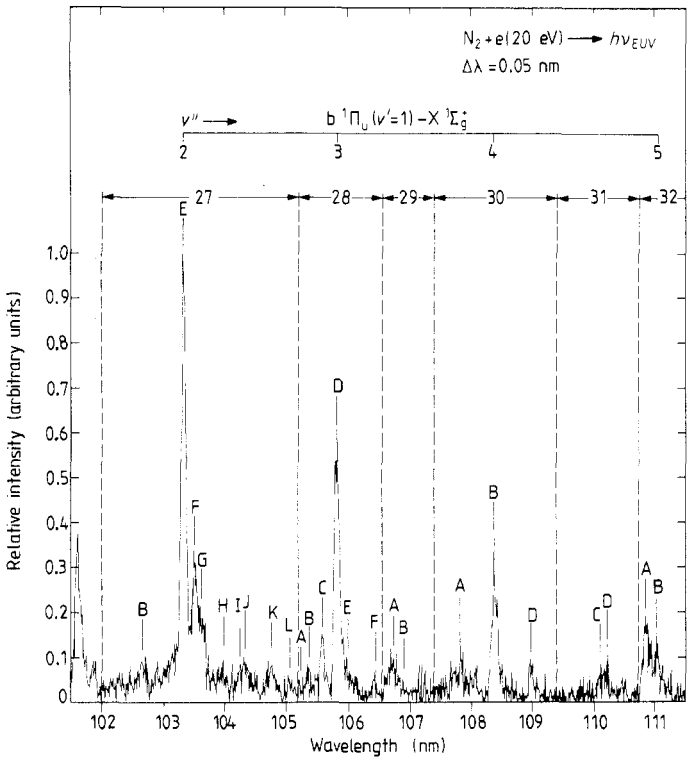

Figure 3. Same as figure 1 above for electron impact at 20 eV. Note the absence of N I, N II lines.

In addition we have measured the excitation function (0–400 eV) for the dominant N II transition at 108.5 nm with 0.5 nm resolution, as shown in figure 6.

Detailed analysis and discussion of the spectral data is presented in the following sections.

4. Analysis and discussion

4.1. Medium resolution spectrum

The main focus of this paper is an analysis of the b $^1\Pi_u$–X $^1\Sigma_g^+$ band system of N_2. However, the emission spectrum measured here in the range 102 to 134 nm also contains contributions from the b′ $^1\Sigma_u^+$–X $^1\Sigma_g^+$ and c_4' $^1\Sigma_u^+$–X $^1\Sigma_g^+$ band systems, together with some LBH bands and many N I and II features.

Emission features corresponding to nine non-resonance bands of the b′ $^1\Sigma_u^+$–X $^1\Sigma_g^+$ system are listed in table 1. The observed features are, in most cases, a blend of several possible spectral components, including N I lines, in the integrated wavelength interval. In order to partition the measured emission cross section of each feature into the various candidate emission channels we employ the following criteria.

(i) N I lines will not be observed in the spectum measured at 20 eV impact energy. Some features, such as 27J, contain a candidate b′–X band blended with N I lines. In these cases the 100 eV cross section for the b′–X component is determined from the

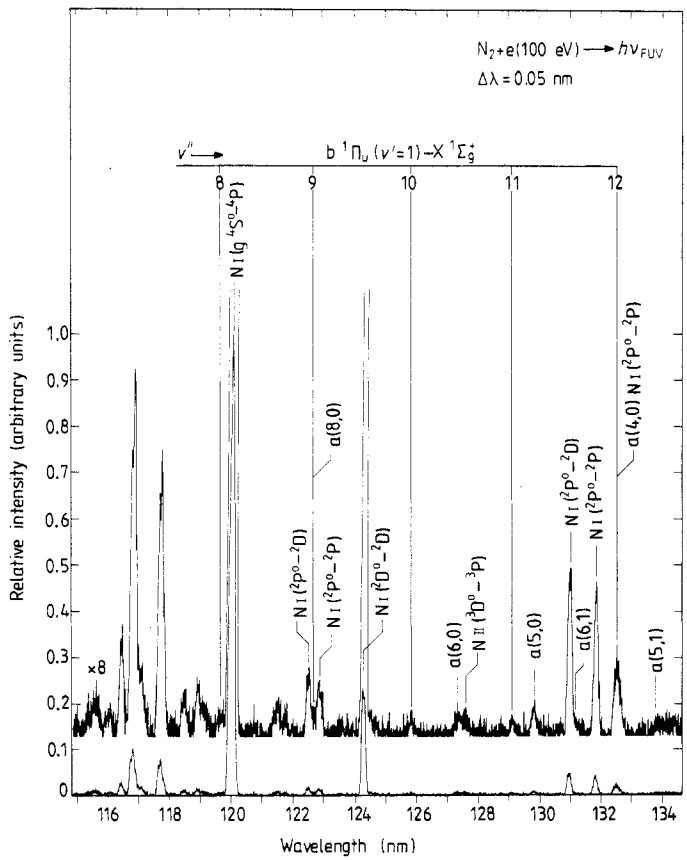

Figure 4. Calibrated optically thin emission spectrum of N_2 from 116 to 134 nm produced by electron impact at 100 eV, measured at 0.05 nm resolution. The b $^1\Pi_u$ (v' = 1)–X $^1\Sigma_g^+$ progression (v'' =8–12) is indicated, together with N I, N II and LBH features in this wavelength interval.

20 eV spectrum in conjunction with the excitation function measurement for the b′–X (16,0) band by Ajello *et al* (1989) which yields a ratio of 0.30 for the 20 eV to 100 eV cross sections.

(ii) The measured thermal rotational energy level emission peaks ($J_{max} \sim 7$) must lie within 0.05 nm of the published band origins of Roncin *et al* (1987).

(iii) For non-resonance transitions the relative intensities of the high-resolution (0.0008 nm) discharge measurements of Roncin *et al* (1987) which separate components otherwise blended in our spectra will be correlated to the expected electron impact band intensities.

Equivalent criteria are applied to the emission features listed in table 1 which contain bands of the $c_4' \, ^1\Sigma_u^+$–X $^1\Sigma_g^+$ system.

The estimated emission cross sections for these b′, $c_4' \, ^1\Sigma_u^+$–X $^1\Sigma_g^+$ bands are incorporated and discussed in the earlier work of Ajello *et al* (1989) which concentrates on the b′ and c_4' states of N_2. The b′–X bands observed in the region from 102 to 123 nm contribute approximately 12% of the total b′–X system emission cross section at 100 eV. The c_4'–X bands in this spectral region, on the other hand, contribute less

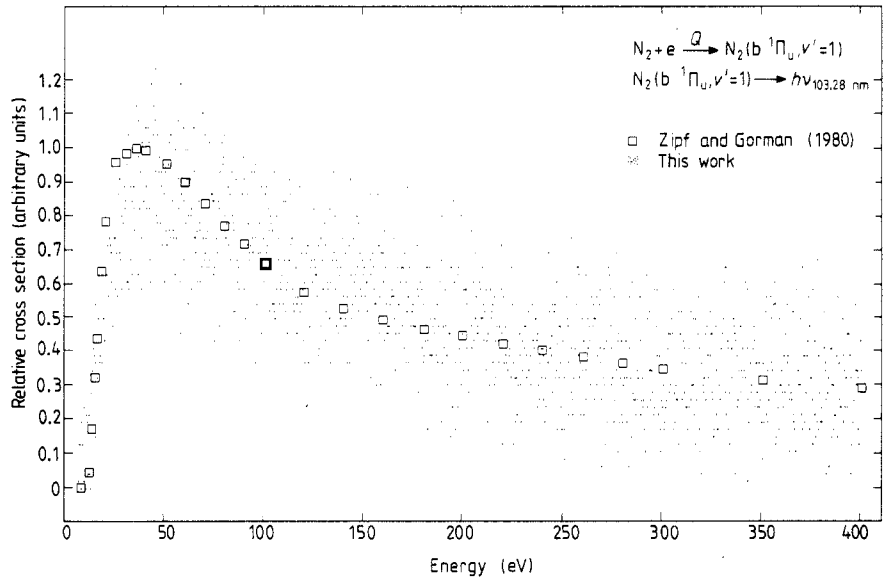

Figure 5. Relative emission cross section of the b $^1\Pi_u$ (1,2) band at 103.28 nm measured from 0–400 eV at 0.086 nm resolution. Data points are taken every 0.4 eV. The measurement of Zipf and Gorman (1980) is overplotted (squares).

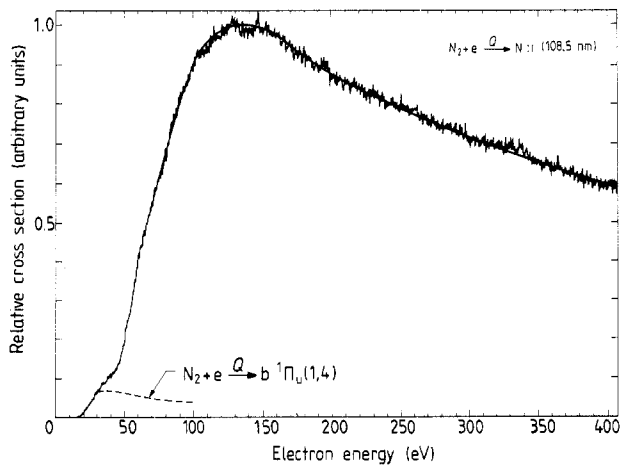

Figure 6. Relative emission cross section of the N II g ^3P–$^3D^o$ multiplet at 108.5 nm, measured from 0–400 eV at 0.5 nm resolution. The estimated contribution of the blended b (1,4) band to the measured cross section is indicated. Data points are taken every 0.4 eV.

than 2% of the total c_4'–X system emission cross section at 100 eV.

Table 2 is a summary of the emission cross sections measured at 100 eV for the $b\ ^1\Pi_u$–$X\ ^1\Sigma_g^+$ band system which spans the observational wavelength range of both this work and Ajello *et al* (1989). The emission spectrum is dominated by the $v' = 1$ progression ($v'' = 0$–12). The only other b–X features observed in this emission study were the (6,3) and (7,5) bands. Other non-resonance emission bands were observed

Table 2. Analysis of $b\,^1\Pi_u$–$X\,^1\Sigma_g^+$ emission cross section at 100 eV.

v'	v''	λ (nm) band origin	Feature	Main blended component	Q_{em} (10^{-19} cm^2) a	Q_{em} (10^{-19} cm^2) b	Branching ratio a	Branching ratio b
1	0	98.56	25D	c_4' (4,5)	1.19	1.07	0.204	0.126
1	1	100.88	26D		1.18	2.11	0.203	0.248
1	2	103.28	27E	N I lines	1.38	2.11	0.237	0.248
1	3	105.76	28D	b′(3,5) b′(9,7)	0.81	1.39	0.139	0.163
1	4	108.33	30B	N II lines	0.44	0.56	0.076	0.066
1	5	111.00	32B		0.17	0.15	0.029	0.018
1	6	113.76			—	—	—	—
1	7	116.62	35D	N I lines	0	0.05	0	0.006
1	8	119.59	38A		0.16	0.14	0.027	0.016
1	9	122.67			0.16	0.27	0.027	0.032
1	10	125.87			0.12	0.28	0.021	0.033
1	11	129.18			0.12	0.22	0.021	0.026
1	12	132.63		a(4,0), N I lines	0.09	0.16	0.015	0.019
Q_{em} ($v'=1$)					5.82	8.51	1.00	1.00
6	3	101.58	26H		0.09	—		
7	5	105.54	28C		0.22	—		
Total Q_{em}					6.13			

[a] This work
[b] Zipf and Gorman (1980)

in the high resolution discharge spectra of Roncin *et al* (1987) from the $v' = 4$, 5, 6 and 7 levels of the $b\,^1\Pi_u$ state though most of these bands were designated as 'weak' or 'very weak'. These features could not be unambiguously identified in our medium resolution electron impact study. The emission cross section measured at 100 eV for the $v' = 1$ progression ($v'' = 0$–12) was 5.82×10^{-19} cm^2. This represents 95% of the total emission observed for the b–X system.

In order to obtain the emission cross sections for the b–X bands listed in table 2 the estimated contributions of any other blended spectral components were subtracted from the measured cross sections of the observed emission features. In cases where the principal overlap components are b′–X or c_4'–X bands we use the data presented by Ajello *et al* (1989) to partition the total feature cross section. For overlap with N I or N II lines we obtain the 100 eV cross section for the b–X band by extrapolating the 20 eV cross section using the 100 eV/20 eV cross section ratio derived from the excitation function measurement of the b–X (1,2) band at 103.28 nm (figure 5). The cross section for the b–X (1,12) band was obtained using the data of Ajello and Shemansky (1985) to estimate the contribution of the blended LBH a–X (4,0) band, in conjunction with the electron impact emission data of Zipf and Gorman (1980) to extrapolate the b–X (1,12) cross section from the b–X (1,11) measurement which is free of any significant blended spectral components.

The emission cross sections of the b–X bands measured in the electron impact experiment of Zipf and Gorman (1980) are also listed in table 2. These values for the 100 eV cross section were extrapolated form their published cross sections at 200 eV using the excitation function measurement of the b–X (1,2) band to obtain the 100 eV/200 eV cross section ratio. In addition, a correction factor of 0.597 has

been applied to their data which reflects the new calibration standard in the VUV for H Lyman-α from dissociative excitation of H_2 (Ajello *et al* 1988). Even with this correction the emission cross section measured by Zipf and Gorman (1980) for the b–X $v' = 1$ progression is 46% higher than our value of 5.82 x 10^{-19} cm^2. The Zipf and Gorman results are hampered by undocumented measurement intervals and lower spectral resolution (0.083 nm). Overlap with blended spectral components is unknown and may account for this discrepancy. For comparison purposes the emission branching ratios of the two data sets are given in table 2.

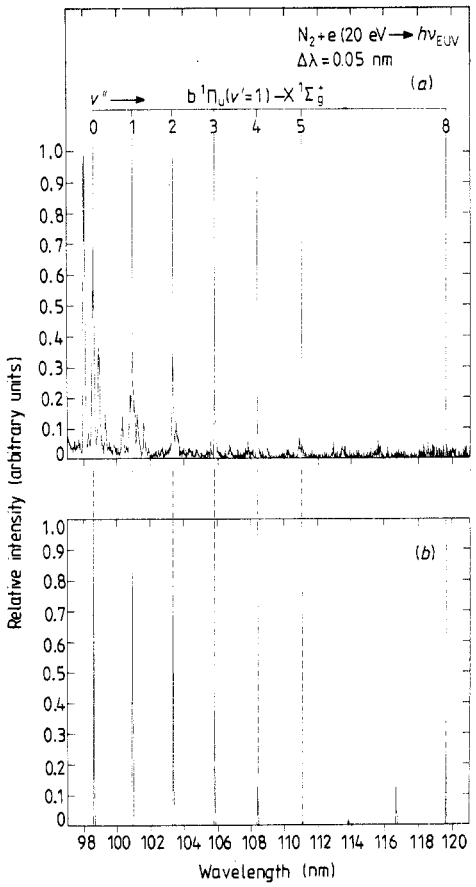

Figure 7. (*a*) Calibrated optically thin emission spectrum of N_2 from 98 to 120 nm produced by electron impact at 20 eV, measured at 0.05 nm resolution. The b $^1\Pi_u$ ($v' = 1$)–X $^1\Sigma_g^+$ progression ($v'' = 0, 1, 2, 3, 4, 5, 8$) is indicated. (*b*) Synthetic spectrum of the b–X $v' = 1$ progression above based on a model of unperturbed Franck–Condon factors to determine branching ratios. The model is convolved with a triangular instrumental slit function at 0.05 nm resolution.

A first-order calculation of the relative intensities within the b–X $v' = 1$ progression based on unperturbed Franck–Condon factors is shown in figure 7, together with the 20 eV emission spectrum measured at 0.05 nm resolution. The synthetic spectrum was generated using the model described by Ajello *et al* (1989). For the unperturbed case, where the electronic transition moment is assumed constant, Franck–Condon

factors were calculated using a Morse potential. Without due consideration of the homogeneous perturbations the agreement between this simple model of branching ratios and the observed $v' = 1$ progression intensities is crude.

Table 3. Analysis of $X\,^1\Sigma_g^+$–$b\,^1\Pi_u$ excitation cross section at 100 eV.

v'	$q_{v'0}$ RKR	$q_{v'0}$ (experimental) Zipf and Gorman (1980)	$q_{v'0}$ (experimental) Geiger and Schröder (1969)	$Q_{v'0}$ (100 eV)[a] Zipf and Gorman (1980) (10^{-19} cm^2)
0	0.0023	0.0092	0.0100	1.1
1	0.0128	0.0533	0.0574	6.5
2	0.0361	0.1193	0.1255	14.4
3	0.0692	0.2228	0.2296	27.0
4	0.1024	0.3543	0.3587	42.9
5	0.1253	0.0183	0.0179	2.2
6	0.1318	0.0168	0.0154	2.0
7	0.1239	0.0950	0.0897	11.5
8	0.1056	0.0019	0.0018	0.24
9	0.0841	0.0191	0.0172	2.3
10	0.0630	0.0565	0.0499	6.8
11	0.0454	0.0190	0.0165	2.3
12	0.0313	0.0043	0.0032	0.52
13	0.0213	—	—	—
14	0.0144	0.0045	0.0032	0.54
15	0.0094	0.0030	0.0021	0.37
16	0.0064	0.0026	0.0018	0.31
17	0.0042			
18	0.0028			
19	0.0019			
Total	1.00	1.00	1.00	121.0

[a] Cross section scaled as indicated in text.

Table 3 shows an analysis of the $X\,^1\Sigma_g^+$–$b\,^1\Pi_u$ excitation cross section at 100 eV. The cross sections ($Q_{v'0}$) are derived from the 200 eV values presented by Zipf and Gorman (1980) from the electron scattering data of Lassettre (1974) and normalised utilising the Lawrence *et al* (1968) oscillator strength value of 0.055 for the (4,0) transition. The total excitation cross section at 100 eV for the $b\,^1\Pi_u$ state ($v' = 0$–16) is 121×10^{-19} cm^2. By comparison the total emission cross section measured for the b–X system at 100 eV is only 6.13×10^{-19} cm^2. The mechanism and importance of this dramatic predissociation of the $b\,^1\Pi_u$ state is discussed in section 4.4. Experimental Franck–Condon factors ($q_{v'0}$) for excitation to the $b\,^1\Pi_u$ $v' = 0$–16 manifold based on the data of both Geiger and Schröder (1969) and Zipf and Gorman (1980) are also listed in table 3. Considerable discrepancies can be seen between these values and the RKR Franck–Condon factors calculated by Stahel *et al* (1983) for the unperturbed $b\,^1\Pi_u$ state.

4.2. Vibrational perturbations

The importance of including the effects of vibrational perturbations in the spectral analysis of the Rydberg and valence states of N_2 is now well established (Ajello *et*

al 1989, Lefebvre-Brion and Field 1986, Stahel *et al* 1983, Carroll and Hagim 1988, Dressler 1969). The structural and intensity irregularities observed in the UV absorption and electron energy loss spectra of the b–X system are known to be due to homogeneous configuration interaction effects between the b $^1\Pi_u$ valence state and the c_n $^1\Pi_u$ and o_n $^1\Pi_u$ Rydberg states. The two approaches that can be used to calculate configuration interaction effects in molecular spectra are the method of coupled equations, and the method of vibronic matrix diagonalisation. These two techniques are summarised by Carroll and Hagim (1988). The matrix optimisation procedure developed by Dressler and co-workers (Dressler 1969, Stahel *et al* 1983) is the most convenient for application to experimental data. Supplemented by the use of coupled equations it provides a basis for the quantitative analysis of the interaction of the b $^1\Pi_u$ and c_3 $^1\Pi_u$ states whose diabatic potential curves cross. Stahel *et al* (1983) have generated diabatic and adiabatic potential curves and performed a definitive multi-level deperturbation analysis of the (b, c, o) $^1\Pi_u$ manifold of states.

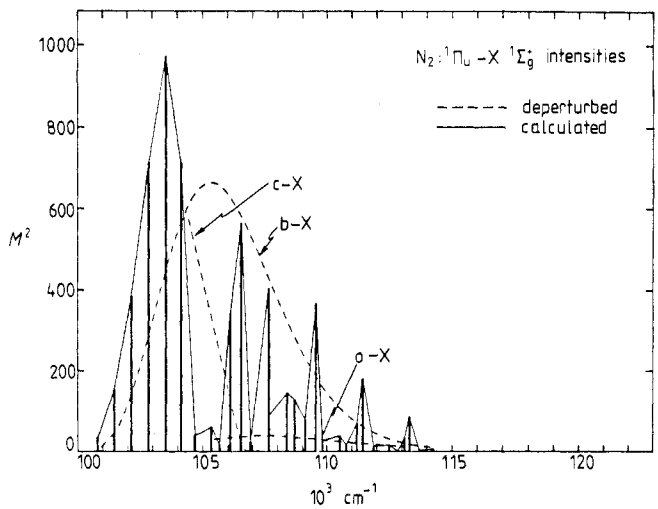

Figure 8. Calculated intensities for N_2 $^1\Pi_u$–X $^1\Sigma_g^+$ ($v'' = 0$) vibronic transitions (reproduced from Lefebvre-Brion and Field 1986). Calculated perturbed intensities (full curves) and deperturbed Franck–Condon envelopes (broken curves) are from Stahel *et al* (1983). Note the interference effect between the b and c states near 105 000 cm^{-1}.

Figure 8 (taken from the monograph of Lefebvre-Brion and Field 1986) is an illustration of the interference effects calculated by Stahel *et al* (1983). Dipole strengths M^2 (proportional to the square of the transition moment) were plotted for the N_2 $^1\Pi_u$–X $^1\Sigma_g^+$ ($v'' = 0$) transitions. The intensity distributions within the vibrational progressions ($v'' = 0$) calculated by Stahel *et al* (1983) for the deperturbed states are represented by the Franck–Condon envelopes shown as broken curves in figure 8. The perturbed intensities calculated by Stahel *et al* (1983) are shown as full vertical lines. Interference between the transition moments of c_3–X (0,0) and the b–X (v',0) progression enhances the bands below and attenuates the bands above the c_3 (0) resonance position at $\sim$ 104 140 cm^{-1}. The intensity distribution of the b $^1\Pi_u$ bands in this energy region resembles a large scale Beutler–Fano-type profile. The destructive interference between b–X and c_3–X transition amplitudes causes particularly strik-

ing attenuation in the band intensities of the nominal b (5,0) and (6,0) bands which would otherwise be at the peak of the deperturbed Franck–Condon intensity distribution. Comparison of the perturbed intensities calculated by Stahel *et al* (1983) with the energy loss data of Geiger and Schröder (1969) shows general agreement between theory and experiment. Stahel *et al* (1983) suggested that some of the discrepancies between observed and predicted band strengths may arise from not including the effects of nuclear rotation in their calculations.

4.3. Cross section energy dependence

The excitation function for the b–X (1,2) band at 103.28 nm has been measured from 0–400 eV at a resolution of 0.086 nm and is shown in figure 5 overplotted with the scaled data of Zipf and Gorman (1980). A modified Born approximation analytic model (described in detail by Shemansky *et al* 1985a,b) has been applied to their excitation cross section data; the measured relative excitation function from threshold is fitted using a nine-parameter collision strength (Ω) analytic formulation. Relative values of the constants (C_n) used in this model are established by accurately fitting the shape of the experimental excitation function from threshold to the maximum available electron energy. The absolute value of the collision strength is then fixed by the first Born approximation using the measured absorption oscillator strength. The advantage of this model is that the formula is accurate at all energies including the threshold region and can be extended to arbitrary high energy.

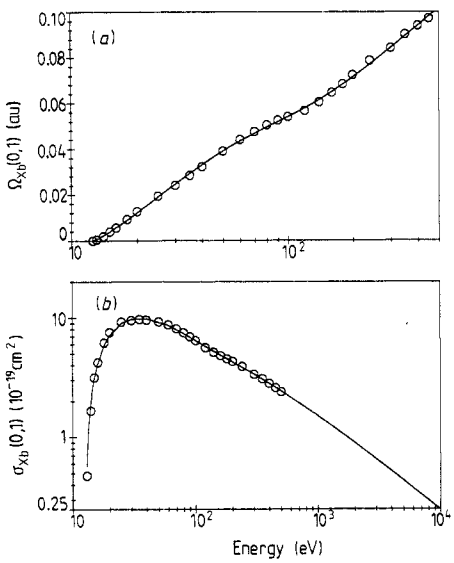

Figure 9. (*a*) Collision strength (Ω) of the b $^1\Pi_u$ $v' = 1$ level from threshold to 500 eV normalised to an oscillator strength of 0.0081 from table 4. Data points (circles) are from Zipf and Gorman (1980); the smooth curve is the analytic fit. (*b*) Excitation cross section of the b $^1\Pi_u$ $v' = 1$ level from threshold to 10 keV. Data points (circles) are from Zipf and Gorman (1980); the smooth curve is the analytic fit.

This can be seen in figure 9 which shows the collision strength and excitation cross section for the $v' = 1$ level of the b $^1\Pi_u$ state from threshold to 500 eV and

Table 4. Tables of molecular parameters for modified Born approximation: N_2 (b–X) molecular parameters. $C_0/C_7 = -0.184\,502$; $C_1/C_7 = 0.522\,830$; $C_2 = C_3 = 0.0$; $C_4/C_7 = 0.654\,255$; $C_5/C_7 = -C_6/C_7 = -0.786\,904$; $C_8 = 0.389\,050$. The values of the emission and excitation cross sections Q_{em} and Q_{ex} are given at 100 eV.

v'	$\bar{\nu}$ (cm^{-1})	$E_{ov'}$ (Ryd)	$q_{v'0}$	$f_{ov'}$	C_7 (au)	Q_{em} (10^{-19} cm^2)	Q_{ex} (10^{-19} cm^2)	η_{pre}
0	100 829.28	0.918 824	0.0091	0.0014	0.005 983	0.00	1.1	1.000
1	101 464.22	0.924 610	0.0528	0.0081	0.034 830	5.82	6.5	0.105
2	102 164.23	0.930 989	0.1186	0.0182	0.078 144	0.00	14.4	1.000
3	102 876.32	0.937 478	0.2219	0.0343	0.146 288	0.00	27.0	1.000
4	103 561.52	0.943 722	0.3537	0.0550	0.233 153	0.00	42.9	1.000
5	104 713.10	0.954 216	0.0184	0.0029	0.012 115	0.00	2.2	1.000
6	105 359.35	0.960 105	0.0169	0.0027	0.011 137	0.09	2.0	0.956
7	106 123.67	0.967 070	0.0958	0.0153	0.063 135	0.22	11.5	0.981
8	106 946.48	0.974 568	0.0020	0.0003	0.001 294	0.00	0.24	1.000
9	107 656.81	0.981 041	0.0194	0.0031	0.012 762	0.00	2.3	1.000
10	108 385.79	0.987 684	0.0574	0.0093	0.037 841	0.00	6.8	1.000
11	109 133.43	0.994 497	0.0193	0.0032	0.012 732	0.00	2.3	1.000
12	109 844.64	1.000 978	0.0044	0.0007	0.002 900	0.00	0.52	1.000
13	110 542.57	1.007 338	0.0000	0.0000	0	0.00	0.00	
14	111 224.15	1.103 549	0.0046	0.0008	0.003 009	0.00	0.54	1.000
15	111 886.63	1.019 686	0.0031	0.0005	0.002 058	0.00	0.37	1.000
16	112 522.67	1.025 382	0.0027	0.0004	0.001 751	0.00	0.31	1.000
Total			1.00	0.156		6.1	121.0	0.949

10 keV respectively; the data points (circles) are from Zipf and Gorman (1980) scaled by the Lawrence *et al* (1968) f_{04} value, and the smooth curve is the analytic fit. Note the high degree to which the model and data fit in the vicinity of the threshold region as well as at high energy. The fit to the excitation cross section has been extended beyond the last data point at 500 eV to 10 keV. Table 4 lists a summary of emission and excitation cross sections, fitting parameters (C_n) and predissocation yields (η) for each vibrational level of the b state. Energy values are from Stahel *et al* (1983). With this information it is possible to construct for any vibrational level and impact energy the emission and excitation cross sections for modelling laboratory and planetary atmosphere data. The values of the oscillator strengths ($f_{ov'}$) derived using this modified Born approximation model are also listed separately in table 5, together with the values calculated by Zipf and Gorman (1980). We obtain a total system oscillator strength of 0.156 for the b state ($v' = 0$–16), compared with the value 0.283 obtained by Zipf and Gorman (1980). We have calculated the absolute excitation cross section on the basis of the Lawrence *et al* (1968) measurement of the f_{04} oscillator strength (table 4). This selection is made on the argument that the Lawrence *et al* absorption measurement was more direct and straightforward than the low resolution (40 meV, 0.3 nm) electron energy loss measurement of Lassettre *et al* (1974). Furthermore, excellent agreement was found between the results presented by Ajello *et al* (1989) and the absolute oscillator strength measured by Lawrence *et al* (1968) for the case of the c_4'–X (0,0) transition. The cross sections calculated on this basis indicate that the N_2 b $^1\Pi_u$ ($v' = 1$) level (table 4) has a predissociation branch of $\eta_{pre} \sim 0.1$, while the remaining levels are mainly predissociative, with $\eta_{pre} > 0.95$. The predissociation fraction of $v' = 1$ indicates on the basis of our data that within 10% the Lawrence *et al* (1968) result represents the lowest possible f value

for compatability of the two data sets. An f value smaller by more than 10% of the Lawrence *et al* value of 0.055 for the (4,0) transition would produce an excitation cross section smaller than the emission cross section at $v' = 1$.

Table 5. Summary of absorption oscillator strengths of $b\,^1\Pi_u$–$X\,^1\Sigma_g^+$ ($v'' = 0$) transitions.

	f_{abs}			
v'	Lawrence *et al* (1968)	Geiger and Schröder (1969)	Zipf and Gorman (1980)	This work[a]
0			0.00239	0.0014
1			0.0139	0.0081
2			0.0311	0.0182
3	0.02 ± 0.01	0.035[a]	0.0579	0.0343
4	0.055 ± 0.011	0.055[a]	0.0922	0.0550
5			0.00473	0.0029
6			0.00437	0.0027
7			0.0248	0.0153
8			0.000506	0.0003
9			0.0276	0.0031
10			0.0146	0.0093
11			0.00439	0.0032
12			0.00126	0.0007
13			—	—
14			0.00131	0.0008
15			0.000887	0.0005
16			0.000752	0.0004
Total			0.283	0.156

[a] Normalised to the Lawrence *et al* absolute value for $v' = 4$.

The wavelength range of this study includes many strong emission features assigned to N I and N II multiplets in table 1, the two most intense being N I g $^4S^o$–^4P and N II g ^3P–$^3D^o$ at 119.99 and 108.5 nm, respectively. We have measured the excitation function for the N I multiplet in an earlier publication (Ajello and Shemansky 1985). The excitation function from 0–400 eV for the N II multiplet at 108.5 nm has been measured at 0.5 nm resolution and is shown in figure 7, together with the estimated contribution of the b–X (1,4) band that is blended into this low resolution measurement. The relative cross section can be put on an absolute scale by normalising to the 100 eV cross section data listed in table 1, yielding a peak cross section of 28.9×10^{-19} cm^2 at approximately 130 eV. The N II multiplet at 108.5 nm is one of the major transitions in the dissociative ionisation of N_2 as well as the direct excitation of N^+ and is an important diagnostic for N^+.

4.4. Predissociation

The $b\,^1\Pi_u$ state, which lies above the $N(^4S) + N(^4S)$ and $N(^4S) + N(^2D)$ dissociation limits, is an interesting example of predissociation in diatomic molecules (Lefebvre-Brion and Field 1986). The predissociation is strong enough to produce appreciable diffuseness in the absorption bands of the $v' = 0$, 2, 3 and 4 levels observed by Carroll and Collins (1969), particularly for the (3,0) band. By contrast the (1,0) band remained relatively sharp. Comparison of the excitation and emission cross section

data in table 4 yields the predissociation to radiation branching ratio (η) for each vibrational level of the b state. With the exception of the $v' = 1$ level ($\eta \sim 0.1$) all other vibrational levels are strongly predissociated ($\eta > 0.95$); the total predissociation yield ($v' = 0$–16) is 0.949. This effect is such that predissociation of the b $^1\Pi_u$ state contributes approximately 6% of the total dissociation cross section of N_2 by electron impact at 100 eV (Winters 1965). The mechanism of this predissociation process has been discussed by Lefebvre–Brion and Field (1986), Leoni and Dressler (1971), Carroll and Collins (1969), Dressler (1969), Ubachs *et al* (1989) and Robbe (1978). Leoni and Dressler (1971) performed the first quantitative analysis of predissociation linewidths by fitting computed band profiles to photoelectric scans of the absorption bands for each vibrational level over a wide range of pressures. The direct (spin–orbit) predissociation mechanism, originally suggested by Carroll and Collins (1969) and Dressler (1969), involving the interaction between the b $^1\Pi_u$ state and the continuum of the C′ $^3\Pi_u$ state was able to explain the observed broadening of the $v' = 0$ and 2 levels and the sharpness of the $v' = 1$ level based on vibrational overlap considerations. The unusually large width of the $v' = 3$ level, however, could not be explained. An accidental (or indirect) predissociation mechanism for the $v' = 3$ level was suggested by Leoni and Dressler (1971) in which the b $^1\Pi_u$ $v' = 3$ level interacts with the dissociative C′ $^3\Pi_u$ state via the nearby diffuse F $^3\Pi_u$ $v' = 0$ level. An alternative explanation by Robbe (1978) suggests that the intermediate predissociated perturbing level in this indirect predissociation process is, in fact, C $^3\Pi_u$ $v' = 8$. These two interpretations are discussed at length by Ubachs *et al* (1989) who have recently determined 'predissociation lifetimes ($\tau_{v'}$)' corresponding to the reciprocal of the predissociation probability for the lower vibrational levels of the b $^1\Pi_u$ state ($v' = 0$–5) from accurate linewidth measurements of multiphoton ionisation spectra. Their measured 'predissociation lifetimes': $\tau_0 = 16 \pm 3$ ps, $\tau_1 > 150$ ps, $\tau_2 = 10 \pm 2$ ps, $\tau_3 = 1.6 \pm 0.3$ ps, $\tau_4 = 9 \pm 2$ ps and $\tau_5 > 150$ ps, correspond to predissociation probabilities ranging from less than 6.7×10^9 s^{-1} for $v' = 1$ to 6.25×10^{11} s^{-1} for $v' = 3$.

Fox and Victor (1988) have recently reviewed electron energy deposition processes in N_2. The understanding of these processes is essential for modelling planetary atmospheric phenomena (Ajello *et al* 1989, Strobel and Shemansky 1982). Predissociation is an important channel for electron energy loss in their modelling. Calculation of the predissociation cross section relies on the availability of both accurate emission and excitation cross sections. Furthermore, knowledge of the final states of the products in the total dissociation cross section measurements of Winters (1965) is essential to avoid 'double counting' when assigning cross section data (Fox and Victor 1988). The total dissociation cross section of N_2 at 100 eV[4] is 2×10^{-16} cm^2; our estimate of the predissociation cross section of the b $^1\Pi_u$ state at 100 eV is 115×10^{-19} cm^2. Thus predissociation of the b $^1\Pi_u$ state, an important source of metastable N(^{2}D) atoms, accounts for approximately 6% of the dissociation of N_2 at 100 eV. The revised emission cross sections for the b $^1\Pi_u$, b′ $^1\Sigma_u^+$ and c$_4'$ $^1\Sigma_u^+$ states reported in this work and by Ajello *et al* (1989) may necessitate the revision of many of the results presented by Fox and Victor (1988), as discussed by Ajello *et al* (1989). Table 6 shows a summary of the excitation, emission and estimated predissociation cross sections of the five Rydberg and valence states of N_2 at 100 eV. The cross section values for the b $^1\Pi_u$, b′ $^1\Sigma_u^+$ and c$_4'$ $^1\Sigma_u^+$ states have already been discussed in this work and by Ajello *et al* (1989). Although weak emissions have been reported from the c $^1\Pi_u$ and o $^1\Pi_u$ states by Roncin *et al* (1987) we are unable to detect emission in our spectra. The excitation

cross sections for these latter two states were extrapolated from the relative intensity measurements of Geiger and Schröder (1969). We estimate that predissociation of the (c'_4, b', b, c and o) manifold of singlet states contributes approximately 23% to the total dissociation cross section N_2 at 100 eV.

Table 6. Summary of Rydberg and valence states. The excitation, emission and predissociation cross sections are abbreviated as Q_{ex}, Q_{em} and Q_{pre}, respectively.

	Q_{ex}		Q_{em}	Q_{pre}
	Absolute 100 eV (10^{-19} cm^2)	Relative[a] 25 keV (10^{-19} cm^2)	Absolute 100 eV	Absolute 100 eV (10^{-19} cm^2)
$c'_4\,{}^1\Sigma_u^+$ (0–7)	121[b]	2987	121[b]	0
$b'\,{}^1\Sigma_u^+$ (0–25)	128[b]	1981	19.9[b]	108
$b^1\Pi_u$ (0–16)	121[c]	2788	6.1[e]	115
$c^1\Pi_u$ (0–7)	161[d]	1588	0[e]	161
$o^1\Pi_u$ (0–5)	75[d]	739	0[e]	75
Total	606		147	459
Total dissociation[f] 100 eV (All states) =	2×10^{-16}			

[a] Geiger and Schröder (1969)
[b] Ajello *et al* (1989)
[c] Zipf and Gorman (1980) (corrected as indicated in the text)
[d] Extrapolated from Geiger and Schröder (1969)
[e] This Work
[f] Winters (1965)

Acknowledgments

This work was supported by the Air Force Office of Scientific Research (AFOSR), the Aeronomy Program of the National Science Foundation (grant number ATM 8715709), and NASA Planetary Atmospheres and Astronomy/Astrophysics Program Offices under contract NAS7–100 to the Jet Propulsion Laboratory, California Institute of Technology, Pasadena, CA 91109, and NAGW to the University of Arizona, Tucson, AZ 85721. We have greatly benefited from careful readings of the manuscript by F Launay, J-Y Roncin and K Dressler.

Note added in proof. Differences from other recent results. We note that a recent derivation of the lifetime of the N_2 $c'_4(3)$ level by Kam *et al* (1989) from experimental emission line shapes is in conflict with the magnitude of the excitation cross sections obtained by the same method applied in the present work (Ajello *et al* 1989). If the Kam *et al* (1989) result is assumed correct, the implication (crudely stated) is that excitation cross sections of the N_2 c'_4 state are a factor of ~ 3 larger than the values derived by Ajello *et al* (1989). This would have the effect of invalidating a large number of related cross section measurements including the results reported in the present paper. We argue that the Kam *et al* (1989) derived lifetime is in conflict with all of the other related (published) experimental measurements and it is very unlikely that their small value can be supported against the weight of evidence. This issue will be discussed in a forthcomming letter.

References

Aarts J F M and De Heer F J 1971 *Physica* **52** 45
Ajello J M, James G K, Franklin B O and Shemansky D E 1989 *Phys. Rev.* A **40** 3524
Ajello J M and Shemansky D E 1985 *J. Geophys. Res.* **90** 9845
Ajello J M, Shemansky D E, Franklin B O, Watkins J, Srivastava S, James G K, Simms W T, Hord C W, Pryor W, McClintock W, Argabright V and Hall D 1988 *Appl. Opt.* **27** 890
Birge R T and Hopfield J J 1928 *Astrophys. J.* **68** 257
Carroll P K and Collins C P 1969 *Can. J. Phys.* **47** 563
Carroll P K and Hagim Kh.l 1988 *Phys. Scr.* **37** 682
Dressler K 1969 *Can. J. Phys.* **47** 547
Forand J L, Wang S, Woolsey J M and McConkey J W 1988 *Can. J. Phys.* **66** 349
Fox J L and Victor G A 1988 *Planet Space Sci.* **36** 329
Geiger J and Schröder B 1969 *J. Chem. Phys.* **50** 7
Huschilt J C, Dassen H W and McConkey J W 1981 *Can. J. Phys.* **59** 1893
Kam A W, Lawall J R, Lindsay M D, Pipkin F M, Short R C and Ping Zhao 1989 *Phys. Rev.* A **40** 1279
Kelly R L 1987 *J. Phys. Chem. Ref. Data* **16** 53
Lassettre E N 1974 *Methods of Experimental Physics* vol 3 pt B ed D Williams (New York: Academic) p 868
Lawrence G M, Mickey D L and Dressler K 1968 *J. Chem. Phys.* **48** 1989
Lefebvre-Brion H and Field R W 1986 *Perturbations in the Spectra of Diatomic Molecules* (Orlando, FL: Academic) ch 5 p 265
Leoni M and Dressler K 1971, *J. Appl. Math. Phys.* (ZAMP) **22** 794
Morgan H D and Mentall J E 1983 *J. Chem. Phys.* **78** 1747
Robbe J M 1978 *PhD Thesis* Université des Sciences et Techniques de Lille, France
Roncin J-Y, Launay F and Yoshino K 1987 *Planet. Space Sci.* **35** 267
—— K 1989 *J. Mol. Spectrosc.* **134** 390
Shemansky D E, Ajello J M and Hall D T 1985a *Astrophys. J.* **296** 765
—— 1985b *Astrophys. J.* **296** 774
Stahel D, Leoni M and Dressler K 1983 *J. Chem. Phys.* **79** 2541
Strobel D F and Shemansky D E 1982 *J. Geophys. Res.* **87** 1361
Tilford S G and Wilkinson P G 1964 *J. Mol. Spectrosc.* **12** 231
Ubachs W, Tashiro L and Zare R N 1989 *Preprint*
Wilkinson P G and Houk N B 1956, *J. Chem. Phys.* **24** 528
Winters H F 1965 *J. Chem. Phys.* **44** 1472
Zipf E C and Gorman M R 1980 *J. Chem. Phys.* **73** 813
Zipf E C and McLaughlin R W 1978 *Planet. Space Sci.* **26** 449